

Electrophoretic Deposition and Physicochemical Characterization of Al_2O_3 -NiO Composite Materials

O. Bintou and O. Savadogo*

Laboratoire de Nouveaux Matériaux pour l'électrochimie et l'énergie, Programme de Génie Métallurgique
Département de Génie Chimique, Polytechnique Montréal, CP 6079 Succ Centre-Ville, Montréal, Québec, Canada

Received: June 25, 2014, Accepted: September 20, 2014, Available online: February 15, 2015

Abstract: Al_2O_3 -NiO composites were fabricated by electrophoretic deposition (EPD). Suspensions were prepared from the mixture of Al_2O_3 and NiO powder in a mixed ethanol-water electrolyte and were stabilized with acetic acid. The effects of the NiO content, sintering temperature and the deposition parameters such as the EPD applied voltage and deposition time on the coating weight, microstructure and crystallinity of final composites were studied. Due to the positive charge of Al_2O_3 and NiO in suspension in the mixed ethanol-water solvent, samples were deposited on the cathode and they were not affected by the possible solvent electrolysis. Coatings with defect-free microstructure were then obtained. These investigations have revealed that the deposits weight gain increases linearly with NiO content and their thickness was controlled by adjusting the NiO content and/or the time of the deposition. By increasing NiO content, the distribution of NiO nano-particles in Al_2O_3 matrix became more homogenous forming thereby an interconnected network like-microstructure which inhibits the grain growth of Al_2O_3 . This illustrates clearly the advantage of EPD for the synthesis of Al_2O_3 -NiO particles. XRD studies have revealed that apart from Al_2O_3 and NiO, a cubic nickel spinel ($NiAl_2O_4$) like phase is formed in the Al_2O_3 -NiO composite. The increase of the applied voltage has resulted in a serious reduction of the deposit weight gain and also to the degradation of their microstructures particularly when the NiO content is lower than 40%.

Keywords: Electrophoretic deposition; oxide; particles, Al_2O_3 -NiO nano-composites

1. INTRODUCTION

The demand of high performing oxide composite materials with low cost for various applications is increasing significantly. One the most interest material for various engineering applications is alumina. This is especially due to its availability, high electrical resistance, dielectric proprieties and chemical inertness. However, the brittleness and low toughness of alumina have limited a long time its applications in industry.

In order to overcome this limitation, one of the approaches is to incorporate another phase toughening material to interact with the propagating crack. As more energy is needed to propagate a crack, the resistance of alumina to catastrophic failure is then enhanced. Many toughening materials such as ceramics or metals have been used to improve the toughness of alumina. Among them, metals like nickel incorporation to alumina have attracted much attention

recently. Its addition to this oxide has indeed improved not only its mechanical properties, but also its electrical, optical, thermal and magnetic properties.

Many researchers have investigated this composite material using mainly metal nickel dispersed in Al_2O_3 [1-4]. However, the metallic particles tend often to oxidize after a period of exposure especially in high temperature environments; there is therefore a need to use, semi-metallic or non-metallic particles which have higher temperature stability [5]. In addition, NiO is more appropriate for this application due to its high electrophoretic mobility, rate of deposition, smooth deposits and better control of the gradient profile [6]. NiO is a highly insoluble thermally stable nickel source suitable for optic and ceramic applications. Nickel oxide is very interesting for this application because it has been used in a variety of applications in electronic [7], thin films [8], electrochemical capacitors (EC) [9]. It is low cost, has an excellent durability and electrochemical stability with large span optical density. There are several methods to fabricate NiO and Al_2O_3 based composite in-

*To whom correspondence should be addressed:
Email: oumarou.savadogo@polymtl.ca

cluding conventional powder mixing technique; Spray pyrolysis; chemical and physical vapour deposition (CVD or PVD), sputtering, sol-gel, like thermal and plasma spraying, precipitation approaches and the template synthesis, and electrophoretic deposition (EPD) [3, 10], [11, 12]. Among these methods, EPD is a fairly rapid and inexpensive way capable to producing a dense and uniform coating on substrates with complex geometries. Electrophoretic deposition is a process for ceramics [13] in which colloidal particles such as ceramics suspended in a liquid medium migrate toward the electrode of opposite sign to their charges under the influence of an electric field (electrophoresis) for deposition. EPD was first observed by a Russian scientist Reuss in his experiment with electric field to induce motion of clay particles suspended in water [14]. But the first practical use of this method is patented in the USA in 1933 with the deposition of thoria particles on a platinum cathode for electron tube [15].

EPD is presently used for many applications, such as metals [16], polymers [17], high performance ceramics coatings [18, 19] layered composites [3, 20], functionally graded materials [6, 21] and nanoparticles deposition to produce advanced nanostructured materials [22]. However, there are few reports on Al_2O_3 -NiO composites fabricated EPD technique.

As indicated above, the preparation of $\text{Al}_2\text{O}_3/\text{NiO}$ composite is well known [10, 12, 24]. But the possibility of preparing the $\text{Al}_2\text{O}_3/\text{NiO}$ composite of controlled composition by the method of electrophoretic deposition is new. Until now there is no research development on the electrophoretic co-deposition of Al_2O_3 -NiO from a mixture of ethanol-water solvent on a nickel foil. In particular in electrophoretic deposition of composite compound, there are particular conditions we may identify for an appropriate control of the deposition process as for example getting the same electrophoretic mobility of the two components in the suspension [25]. We have determined previously the electrophoretic mobility of Al_2O_3 and that of NiO in a mixture ethanol-water suspensions stabilized by acetic acid [23]. Accordingly, we have determined the stability and electrophoretic deposition behavior of NiO or alumina, separately, in a mixture of ethanol-water to optimize the deposition conditions of each of these oxides. The objective of the present study was to study, for the first time, the fabrication using electrophoretic deposition of the Al_2O_3 -NiO nano-composite with low content in defects. In particular we report the effect of NiO content on the microstructure, thermal stability and the particular size of the Al_2O_3 -NiO nano composite prepared by EPD.

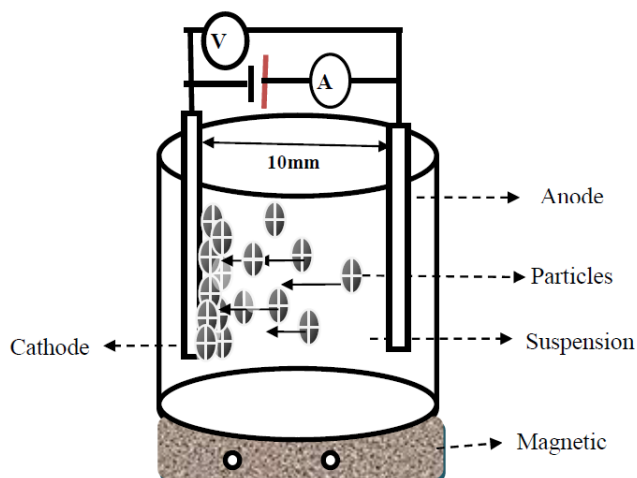


Figure 1. Schematic illustration of EPD experimental Setup

2. EXPERIMENTAL DETAILS

2.1. Material and suspensions preparation and characterization

The alumina and nickel oxide based materials used in this work are similar to those of the preceding work [23]. The alumina powder was from Baikowski International corp, USA. Its crystal structure is 100 % alpha. Its purity is higher than 99.99% with an average particle size of 0.6 μm . Its specific surface area (S_{BET}) was 15 m^2/g and its density was 3.98 g/cm^3 . The nickel (II) oxide was purchased from Sigma-Aldrich, USA. Its particle size was less than 50 nm and its purity 99.8 % and density 6.67 g/cm^3 .

All suspensions were prepared by a mixture of a total mass of 1g. It is composed of the two powders with a varying mass ratio of Al_2O_3 and NiO in 100ml of solvent which is formed of ethanol and water in a ratio of 80-20 in volume. Prior to the film deposition, all the suspensions were magnetically stirred for 15 min and subsequently ultrasonicated in an ultrasonic bath for 24 hours to ensure a good dispersion of the particles. Acetic acid (99%) was used as the stabilizing and dispersing agent. HCl (37%, Fisher Chemicals) adjusted the pH on acid side and NaOH on the basic side. The pH values can range from 2 to 12.

Electrophoretic mobility and the zeta potential (ZP) were meas-

Table 1. Characterization of the suspensions used for electrophoretic deposition of the particle composite

Mixing $\text{Al}_2\text{O}_3/\text{NiO}$ (%)	Potential zeta ζ (mV)	electrophoretic mobility μ ($10^{-8}\text{m}^2(\text{V}\cdot\text{s})^{-1}$)	Suspension conductivity ($\mu\text{S}/\text{cm}$)
S ₁ (85/15)	80.06	1.58	192
S ₂ (75/25)	80.01	1.58	201
S ₃ (60/40)	80.02	1.56	208
S ₅ (50/50)	79.01	1.55	212
S ₆ (40/60)	79.00	1.54	213
S ₇ (30/70)	79.00	1.54	214
S ₈ (20/80)	79.00	1.53	214

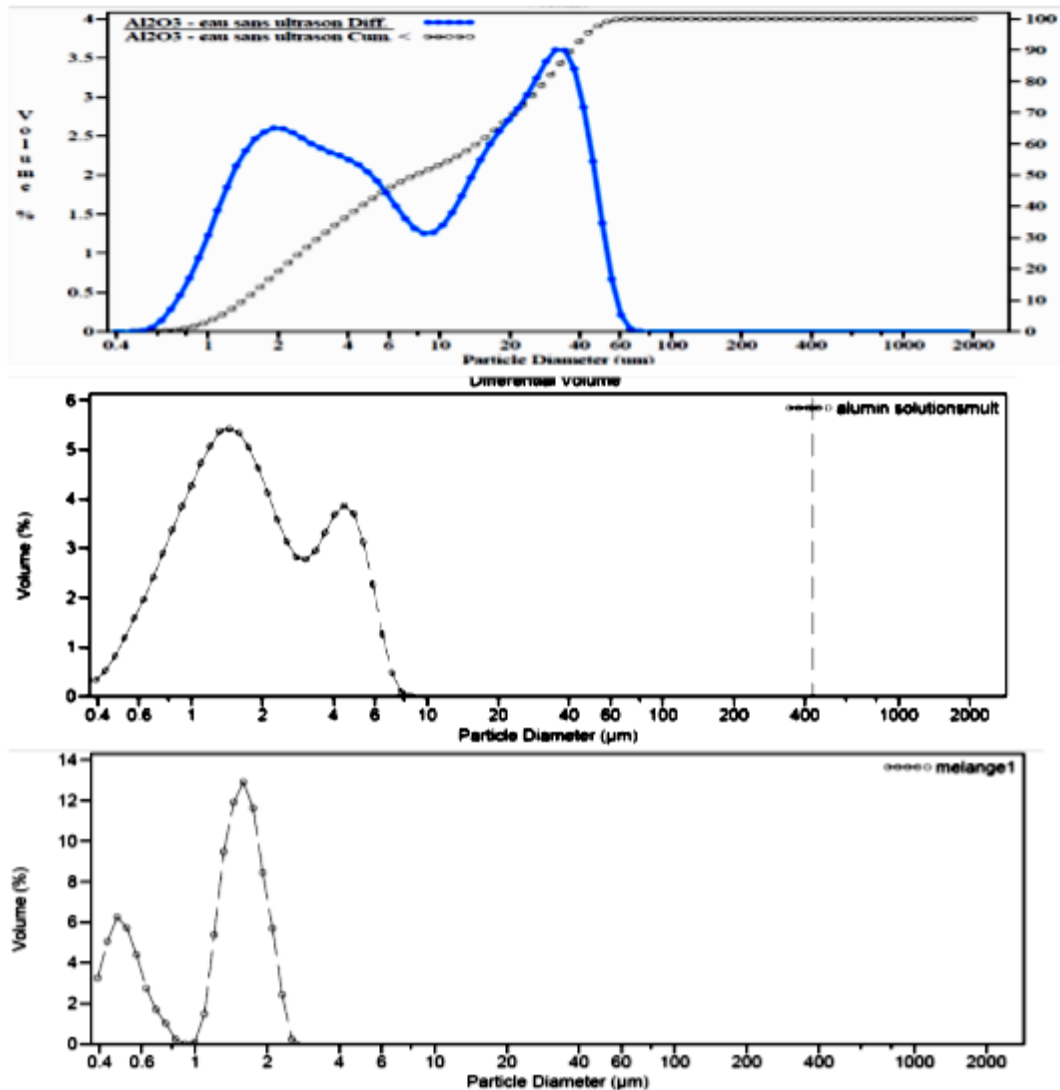


Figure 2. Particle size distribution of Al_2O_3 ((a) and (b)) and mixture $\text{Al}_2\text{O}_3\text{-NiO}$ (c) powder dispersed in de-ionized water.

ured via a Zeta Plus zeta potential analyzer; the pH of the suspensions was measured by means of a pH meter (WTW, 315i) at room temperature ($25.0\text{ }^\circ\text{C} \pm 0.5$). The particle size distribution was measured using laser light diffraction particle size analyzer (LS 230, Coulter-Beckman, Germany). This allows measuring particle sizes from $0.4\text{ }\mu\text{m}$ to $2000\text{ }\mu\text{m}$ by combination of laser light scattering for the determination of the coarse particles and polarization intensity differential scattering (PIDS) for measuring the finer particles. Sedimentation of the particles was investigated in cylinders and by in situ measurements of the particle size distribution with the LS 230. The conductivity of the suspension was measured using an YSI conduct meter.

2.2. EPD deposition parameters and sample characterization

Metallic foils of nickel were used as deposition electrode; the same electrodes with the same dimension were used as the counter

electrode. The electrodes were cleaned with acetone, ethanol and distilled water in an ultrasonic bath for 15 min before the deposition process. The distance between the working and counter electrodes was kept constant (1cm) during the deposition. The mixed ethanol-water solvent containing $\text{Al}_2\text{O}_3\text{-NiO}$ suspensions were prepared by mixing 1g of Al_2O_3 and NiO (NiO content variable of 0 to 100%) in 150ml of mixture ethanol-water. Properties of the suspensions used are summarized in Table 1. The composites were deposited at pH 2.5 with a constant voltage in the range of 150-300 V. After deposition, samples were first dried at room temperature for 24 h, and at $70\text{ }^\circ\text{C}$ for 1 h. The weight gain and the green density of the coatings was evaluated. After drying, they are sintered at temperature ranging from 500 to $1250\text{ }^\circ\text{C}$ for some subsequent studies. During the electrophoretic deposition of the composite, constant voltages was applied across the electrodes yielding variable currents between 10 to 60 mA. During the depositions, the suspensions in the mixed solvents were continually stirred during the

deposition to prevent the sedimentation.

The deposits were sintered at different temperatures in air for 5h. The XRD patterns of the samples were obtained using X Philips X'PERT X-ray powder diffraction (XRD) with $\text{CuK}\alpha$ ($\lambda = 1, 5406 \text{ \AA}$) at a scanning rate of $1.2^\circ/\text{min}$ with 2θ range from 20° to 80° . The microstructural observations and chemical composition of the coatings were obtained using scanning electron microscope SEM JEOL JSM840 energy dispersive spectroscopy (EDS). Prior to SEM analysis, the surfaces of the specimens were polished coated with gold to avoid charging during the SEM observations. The chemical composition of the coating and the nature of the growth were determined using the energy dispersive spectroscopy (EDS).

The particle size of the procured Al_2O_3 and composite powder was analyzed by COULTER® LS Particle Size Analyzer. The powder was dispersed in de-ionized water and stirred magnetically by ultrasonic agitation for 10 min just before the determination of the particle size. Fig. 1 shows the Schematic illustration of the EPD experimental Setup.

3. RESULTS AND DISCUSSION

3.1. Particle size characterization

Fig. 2 shows the particle size distribution of Al_2O_3 (Fig. 2a and 2b) and the composite ($85\%\text{Al}_2\text{O}_3$ - $15\%\text{NiO}$) (Fig. 2c) powder consists of two peaks. The particle size distribution was therefore bi-modal kind and wide in nature. As seen in Fig. 2a, the average particle size is 6 mm which is to be expected as this was the specified particle size from the suppliers. The peaks shown in Fig. 2a are suggesting there is still some agglomeration of particles occurring due to 90% of them has a size distribution more than $20 \mu\text{m}$ (Table 2 and Fig. 2a). However with 10 min ultrasonic, the average particle size of alumina particles is lowered from 0.6 mm to under $0.4 \mu\text{m}$ (Table 2) and 90% of the particles have a size distribution under $5 \mu\text{m}$ in size (Fig. 2b). Fig. 2c shows that with added 15% of NiO, the average particle size is very reducing (under $0.1 \mu\text{m}$) and 90% of $\text{Al}_2\text{O}_3/\text{NiO}$ particles have a size distribution under $2 \mu\text{m}$ in size. This shows that the size of alumina particles can be reduced by ultrasonic stirring and the particle size of the composite is significantly reduced by the addition of NiO particles.

3.2. Effect of nickel oxide content on the composite

3.2.1. The effect of NiO content on composite weight gain

Table 2. LS Particle Size Analyzer

Particles (%)	Particles diameter (mm)		
	Al_2O_3 dispersed in water without ultrasonic	Al_2O_3 dispersed in water with 10 min ultrasonic	$85\text{Al}_2\text{O}_3/15\text{NiO}$ dispersed in water with 10 min ultrasonic
10	0.961	0.750	0.464
25	1.293	1.086	0.606
50	2,008	1.697	1.421
75	4.974	3.180	1.716
90	20.18	4.770	1.975
Mean	6.022	2.263	1.290
Median	2.008	1.697	1.421

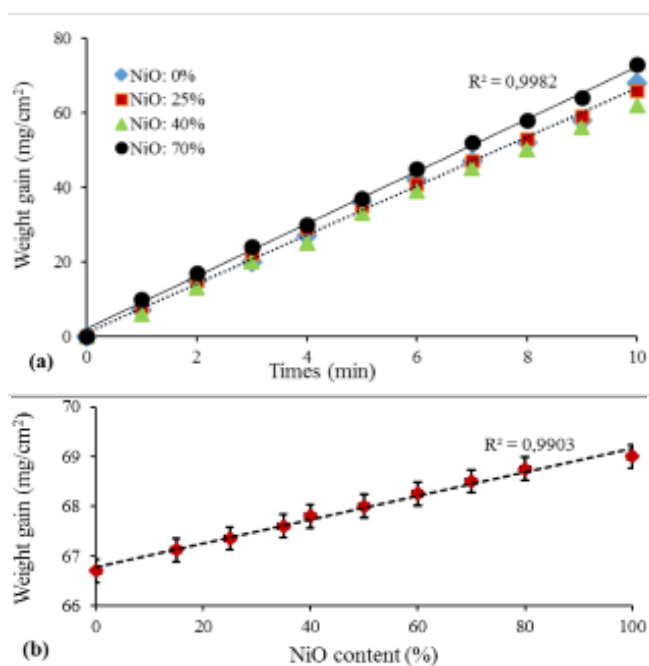


Figure 3. Weight gain of Al_2O_3 -NiO composite deposited at 150 V as a function of the deposition time (a) and the NiO content (b).

Fig. 3a shows the deposition weight gain of Al_2O_3 -NiO composite with different NiO content as a function of deposition time. The results show that the weight of the deposits increases linearly with the deposition time. This is in agreement with the first classical model of Hamaker [24]. This model relates the mass of the film to the deposition parameters as:

$$m = C \cdot \mu_e \cdot E \cdot S \cdot t \quad (1)$$

Where m (g) is the mass of the deposited film, C (g m^{-3}) the suspension concentration, and μ_e ($\text{m}^2 \text{s}^{-1} \text{V}^{-1}$) the electrophoretic mobility system, E (V m^{-1}) is the electric field, S (m^2) is the surface area of the sample, t (s) is the deposition time.

The electrical field can be determined through the relationship between the electric field E , the applied voltage U_{ap} (V), the voltage drop in the deposit U_{dep} (V), and the distance between the two electrodes d (cm).

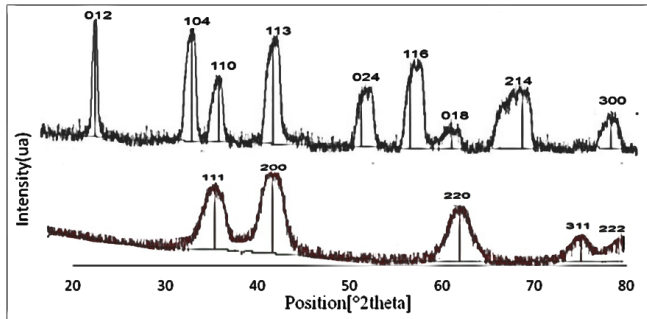


Figure 4. XRD patterns of alumina and nickel oxide powders.

$$E = \frac{U_{ap} - U_{dep}}{d} \quad (2)$$

Considering Eq.(1) and (2), the deposition weight gain W (g/cm²) is determined.

$$\frac{m}{S} = \frac{C \cdot \mu e}{d} \cdot (U_{ap} - U_{dep}) \cdot t = W \quad (3)$$

The mass of the deposit increases with time. This indicates that the film thickness can be controlled easily by adjusting the deposition time.

Fig. 3b shows the variation of the deposition weight gain of the composite deposited for 10 min as a function of the NiO content. These results show that the weight of the deposited composite increased linearly with the NiO content. For example, the weight gains of the composite increases from 67 to 68 mg/cm² when the NiO content increases from 15 to 50 %. The extrapolation of the value of the weight gain at NiO concentration is zero shows clearly that that the weight gain of the Al₂O₃-NiO composite is higher than that of Al₂O₃ alone. Furthermore, this figure suggests that the deposition thickness of the composites could also be controlled by adjusting the NiO content.

3.2.2. The effect of NiO content on the composite crystallite size and orientation

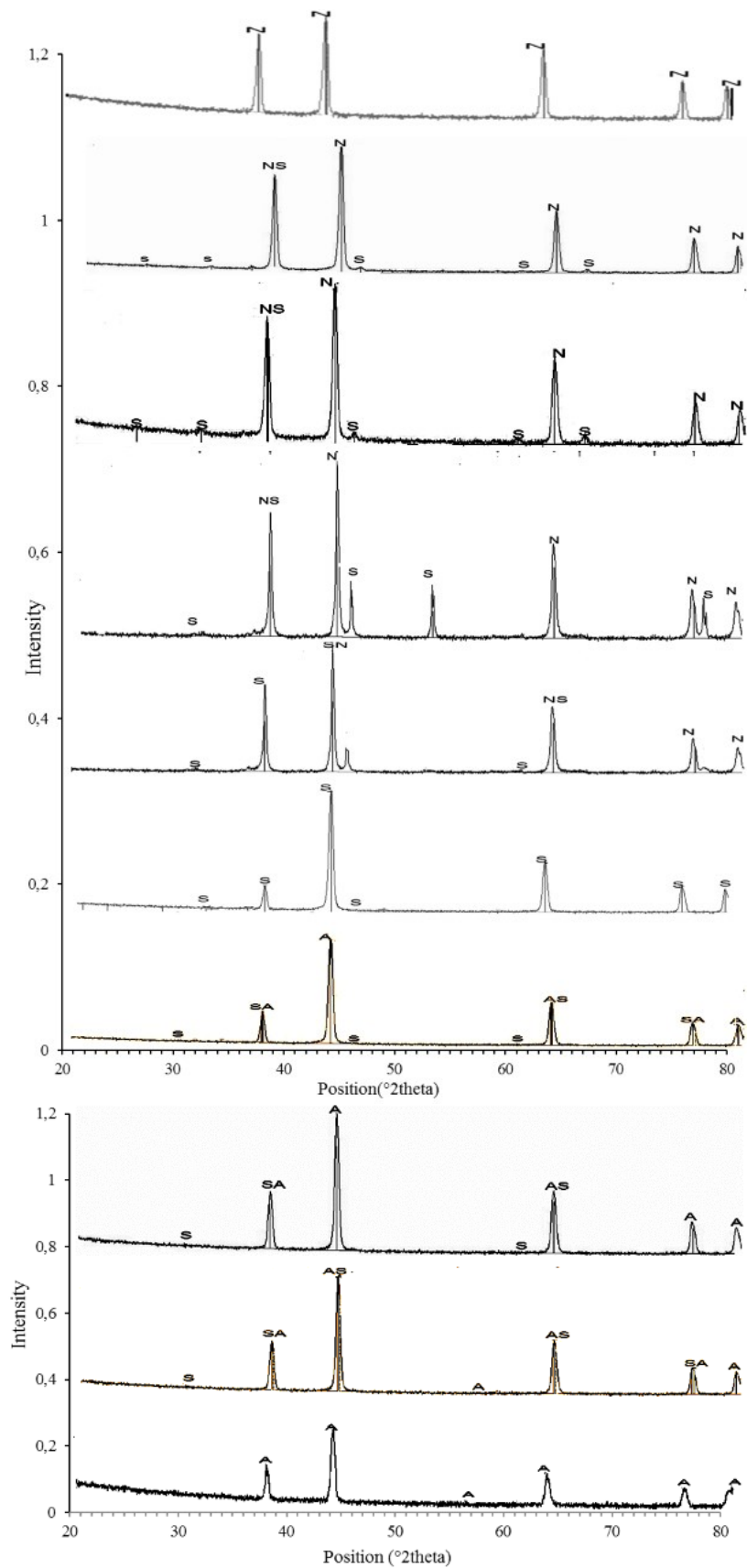
The X-ray diffraction results for pure Al₂O₃ and NiO powder are presented in Fig. 4 and in Table 3 and 4. Fig. 4a clearly shows distinct peaks at 2θ of 37.464, 43.1768, 62.6324, 75.8083, and 78.9872 who have been identified as peaks of the cubic NiO crystallites with various diffracting lines (111), (200), (220), (311) and (222). Fig.4b was identified the presence of α -Al₂O₃ at 2θ (Miller indices) = 25.594°, 35.197°, 37.804°, 43.381°, 52.588°, 57.538°, 61.333°, 66.547°, 68.230°, and 76.909° corresponding to diffraction line (012),(104), (110), (113), (024), (116), (211), (018), (214), (300) respectively. Table 3 and 4 show the full width of diffraction peaks at half-maximum (FWHM) for NiO and Al₂O₃ at various peaks. The crystallite sizes for Al₂O₃ and NiO were evaluated from the FWHM [$^{\circ} 2\theta$.] value using the Scherrer's equation.

Table 3. Experimental XRD data of NiO nanopowder

Pos. [$^{\circ}2\theta$.]	FWHM [$^{\circ}2\theta$.]	d-spacing [Å]	Rel. Int. [%]	Identification (NiO)	Crystallite size (nm)	Average crystallite size (nm)
37.4566	0.3423	2.4015	54.04	(111)	26.10	23.45
43.1768	0.3149	2.0952	100.00	(200)	28.90	
62.6324	0.9446	1.4832	38.28	(220)	10.48	
75.8083	0.7872	1.2548	11.33	(311)	13.62	
78.9872	0.2880	1.2111	8.97	(222)	38.07	

Table 4. Experimental XRD data of Al₂O₃ powder

Pos. [$^{\circ}2\theta$.]	FWHM [$^{\circ}2\theta$.]	d-spacing [Å]	Rel. Int. [%]	Identification (α -Al ₂ O ₃)	Crystallite size (nm)	Average crystallite size (nm)
25.6168	0.1378	3.4775	100.00	(012)	62.97	34.86
35.5993	0.3542	2.5219	57.30	(104)	25.09	
37.1925	0.3149	2.4175	14.47	(110)	28.35	
43.3815	0.1920	2.0669	74.16	(113)	47.43	
52.1493	0.5510	1.7539	19.56	(024)	17.09	
57.5200	0.2362	1.6023	47.34	(116)	40.86	
58.4099	0.2755	1.5800	33.32	(211)	35.18	
62.0010	0.3936	1.4968	4.25	(018)	25.08	
68.2221	0.3149	1.3747	24.92	(214)	3245	
76.1077	0.2362	1.2507	3.53	(300)	45.49	

Figure 5. XRD patterns of $\text{Al}_2\text{O}_3/\text{NiO}$ with varying NiO content.

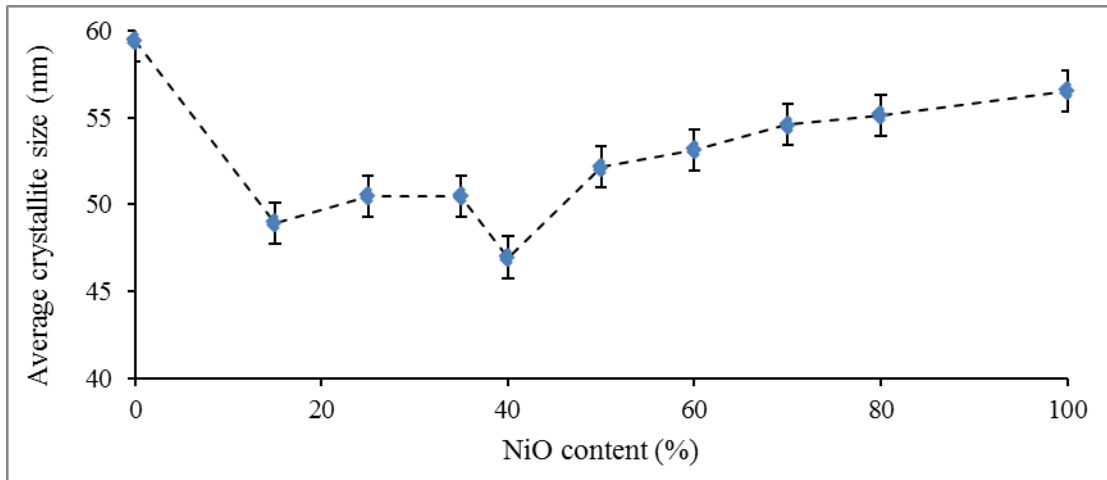


Figure 6. The average crystallite size of composite as function of the NiO content.

$$D = \frac{0.94 \lambda}{FWHM \cdot \cos\theta} \quad (4)$$

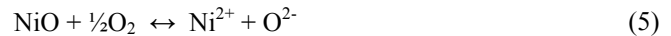
Here D (nm) is the crystallite size, λ is the X-ray wavelength of CuK α radiation (evaluated as 0.154 nm), FWHM in radians stands for full-width of the diffraction line at half-maximum intensity, while θ the diffraction angle. As shown in Table 3 and 4, the crystallite sizes or grain size varied between 10 and 38 nm for NiO and between 17 and 62 nm for α -Al₂O₃. The average crystallite sizes were 23.45 nm for NiO and 34.86 nm for α -Al₂O₃.

Fig. 5a to 5j show the XRD patterns of the Al₂O₃-NiO coatings sintered at 1000 °C in air for 5 h as a function of the NiO content. The XRD patterns of all samples are similar, suggesting that they possess close crystallinity and similar phases. The patterns of Fig. 5a are attributed to those of pure α -Al₂O₃. In this case, only the diffraction peak lines of (110), (113), (018) and (300) were observed. On the other hands, the peaks in Fig. 5j are attributed to those of the cubic phase of the NiO. All the peaks correspond to those of NiO.

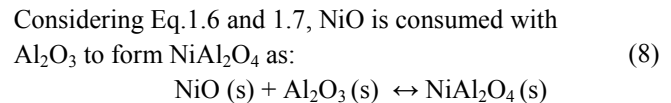
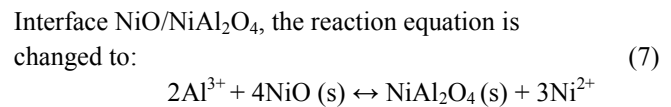
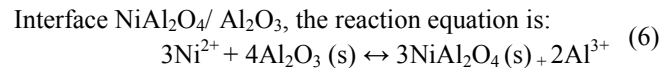
The patterns obtained from Fig. 5b to 5i show that, apart the peaks of Al₂O₃ and NiO, those of NiAl₂O₄ are also observed. The most intense reflection peak for each of the samples prepared at different NiO content correspond to (113) at about 43.3° which indicate a strong preferred orientation. All of the data indicate that the films were polycrystalline and the difference in the peak intensities was indicative of different degrees of crystallinity. After only 15% of NiO was dispersed into the Al₂O₃ matrix, the cubic nickel aluminates spinel phase (NiAl₂O₄) is formed. As more NiO is added, the most intense diffraction peak corresponded to (113) of Al₂O₃ crystalline phase gradually increases in intensity until reaching the maximum after added 40% of NiO, which NiAl₂O₄ spinel becomes the sole phase indicating that NiO has completely diffused into the alumina matrix to form the spinel phase. However, Al₂O₃ and NiAl₂O₄ phase co-existed on the composite as long as the NiO solid fraction added is less than 35%. At very high nickel oxide contents (~50 and more), finally the peaks of NiO phases were detectable generating the presence of mixed phases of NiAl₂O₄ and

NiO on the surface.

XRD analysis suggests that the defect equation as a function of NiO content in Al₂O₃ matrix at 1000 °C in air for 5 hours might be due to the following reactions:



Ni²⁺ could enter the lattice defect to form spinel NiAl₂O₄ structure (Ni²⁺ ion is situated in tetrahedral sites and Al³⁺ in octahedral positions in the cubic closed packing of oxygen anions). In order to preserve local electroneutrality during the reaction through-out the product, it is necessary, for every three Ni²⁺ ions that diffuse to the right hand interface, two Al³⁺ ions must diffuse to the left hand interface. The reaction that occur at the two interfaces may be written as:



The average crystallite sizes of Al₂O₃-NiO coatings were evaluated from the most intense reflections peaks using the Scherrer's equation. Fig. 6 shows the average crystallite size of composite as function of the NiO content. In Fig. 6, the peaks marked as A correspond to Al₂O₃, N to NiO and S to NiAl₂O₄ crystallites. We can see on Fig. 6 that the average grain size of the particles is smaller than those of the Al₂O₃-NiO composite materials. The addition of NiO nanoparticles has therefore restrained the growth of Al₂O₃ grains.

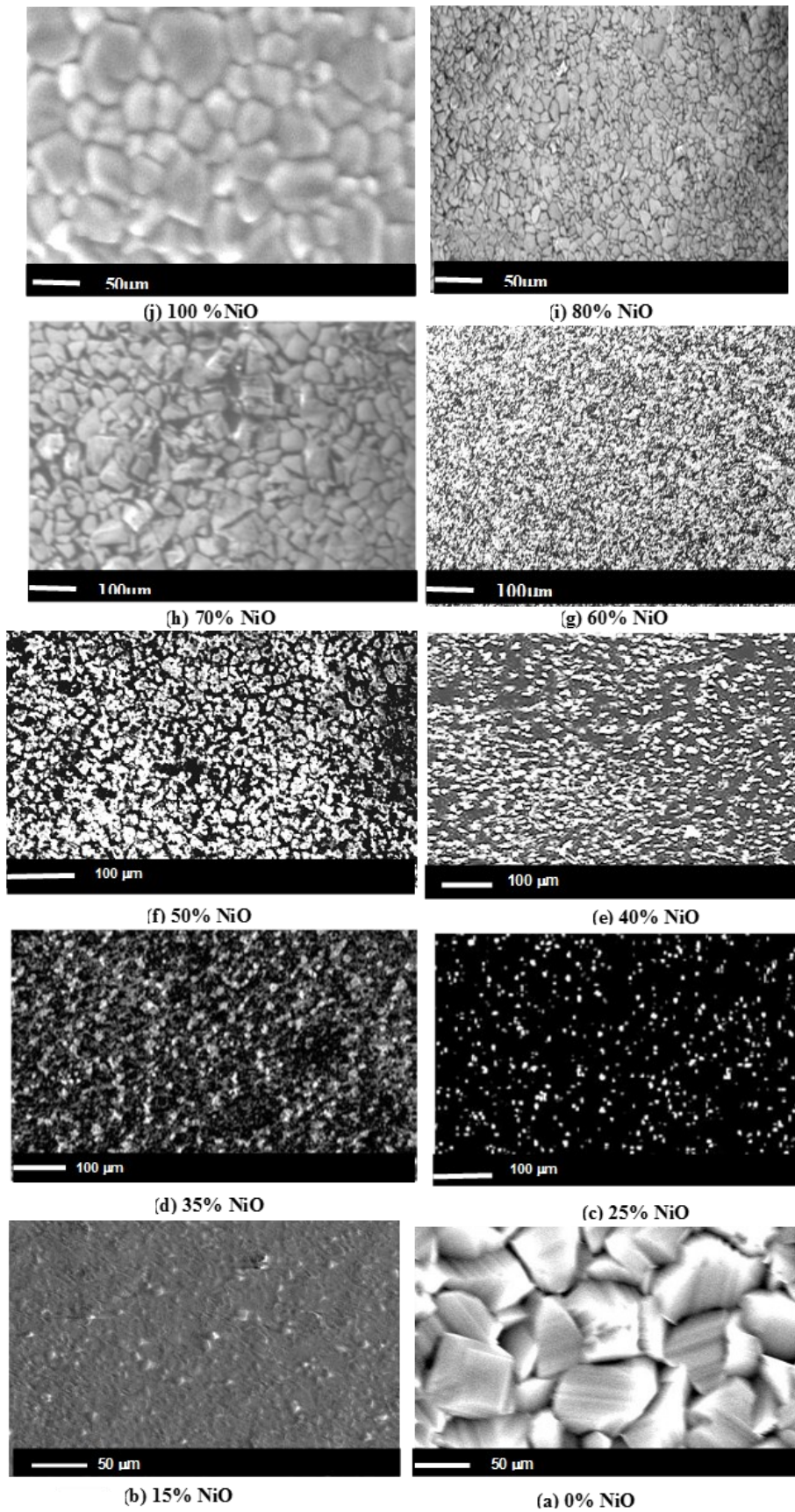


Figure 7. SEM images of Al_2O_3 -NiO with 0 to 100% of NiO content and sintered at 1000 °C (NiO appears as light grey).

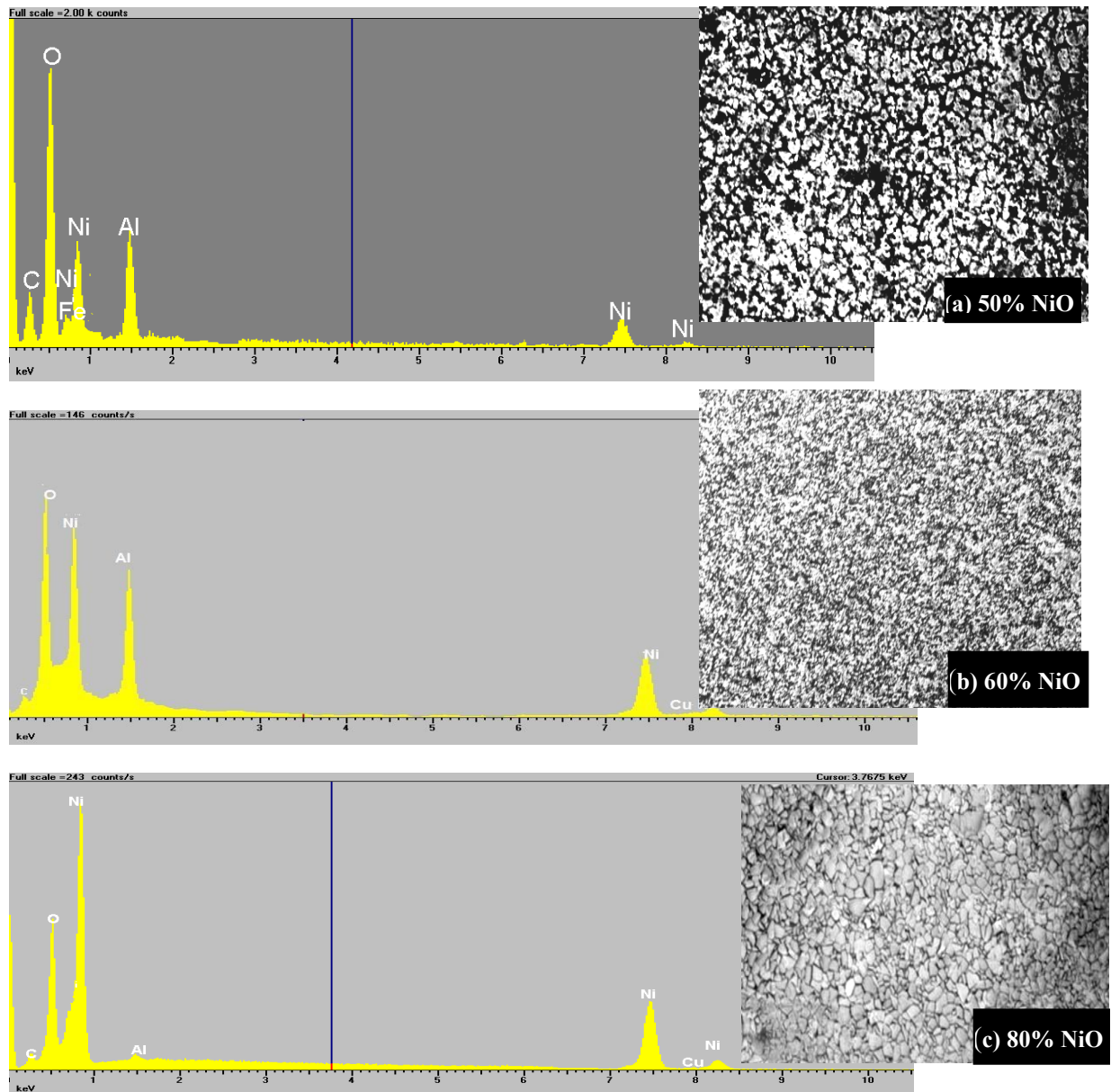


Figure 8. Energy dispersive spectrum of Al_2O_3 -NiO composites sintered at $1000\text{ }^\circ\text{C}$

3.2.3. The effect of NiO content on the composite microstructure and composition

Fig. 7a to 7j show the SEM images of the Al_2O_3 /NiO composites deposited on a Ni substrate and sintered at $1000\text{ }^\circ\text{C}$ for 5h as function of NiO content. In the SEM images of these samples, the color of NiO was light gray and the color of Al_2O_3 was dark. As we can see from Figs. 7b and 7c, NiO particles were distributed mainly on the grain boundaries and triple points of Al_2O_3 matrix, in the form of finely divided and uniformly distributed particles. Furthermore, the microstructures of the composite are uniform. Hence, in this investigation the composite can be defined as inter granular-type. When the content of NiO increases, NiO distribution become more symmetric, and most of them are in contact with one another, form-

ing an interconnected network-like-microstructure which could inhibit the grain growth of Al_2O_3 so as to improve the mechanical properties of the composite, such as fracture toughness. Evidently, the composites have a fine matrix grain size when compared with the monolithic Al_2O_3 (Fig. 2, Fig. 6 and Table 2). A feature important at noting is the uniformity of the NiO phase distribution. The homogeneity increases with increasing the NiO content illustrating the advantage of EPD for the synthesis of these particles composites. The similar microstructure was reported elsewhere in Al_2O_3 -NiO EPD for Functional Grade Materials [6].

To determine the chemical composition of the different phases observed in Fig. 7, energy dispersive spectroscopy (EDS) study was performed on different regions on the coated surface. Individu-

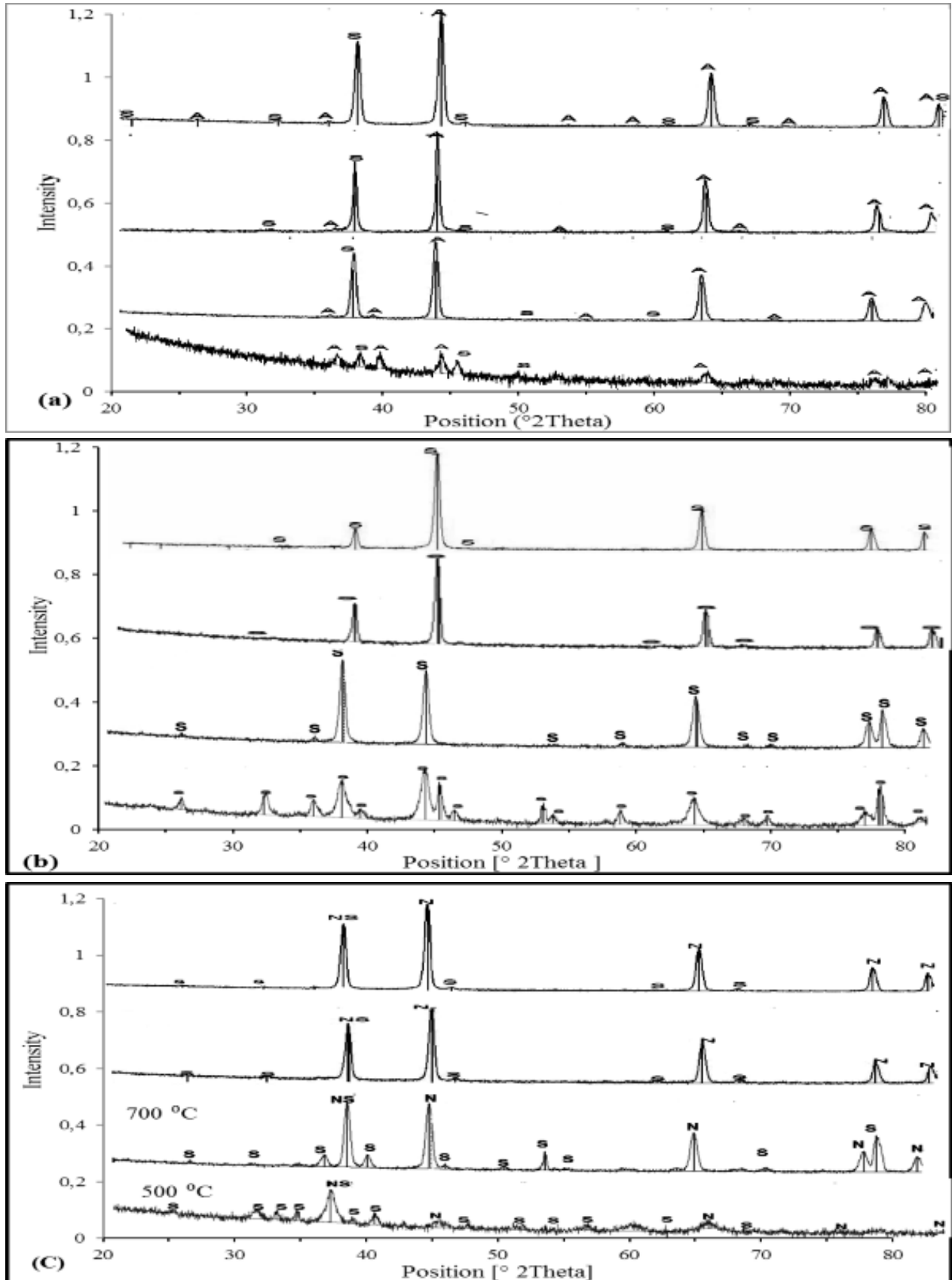


Figure 9. XRD patterns of $\text{Al}_2\text{O}_3\text{-NiO}$ with 25 (a), 40 (b) and 70% (c) of NiO content as a function of the sintering temperature.

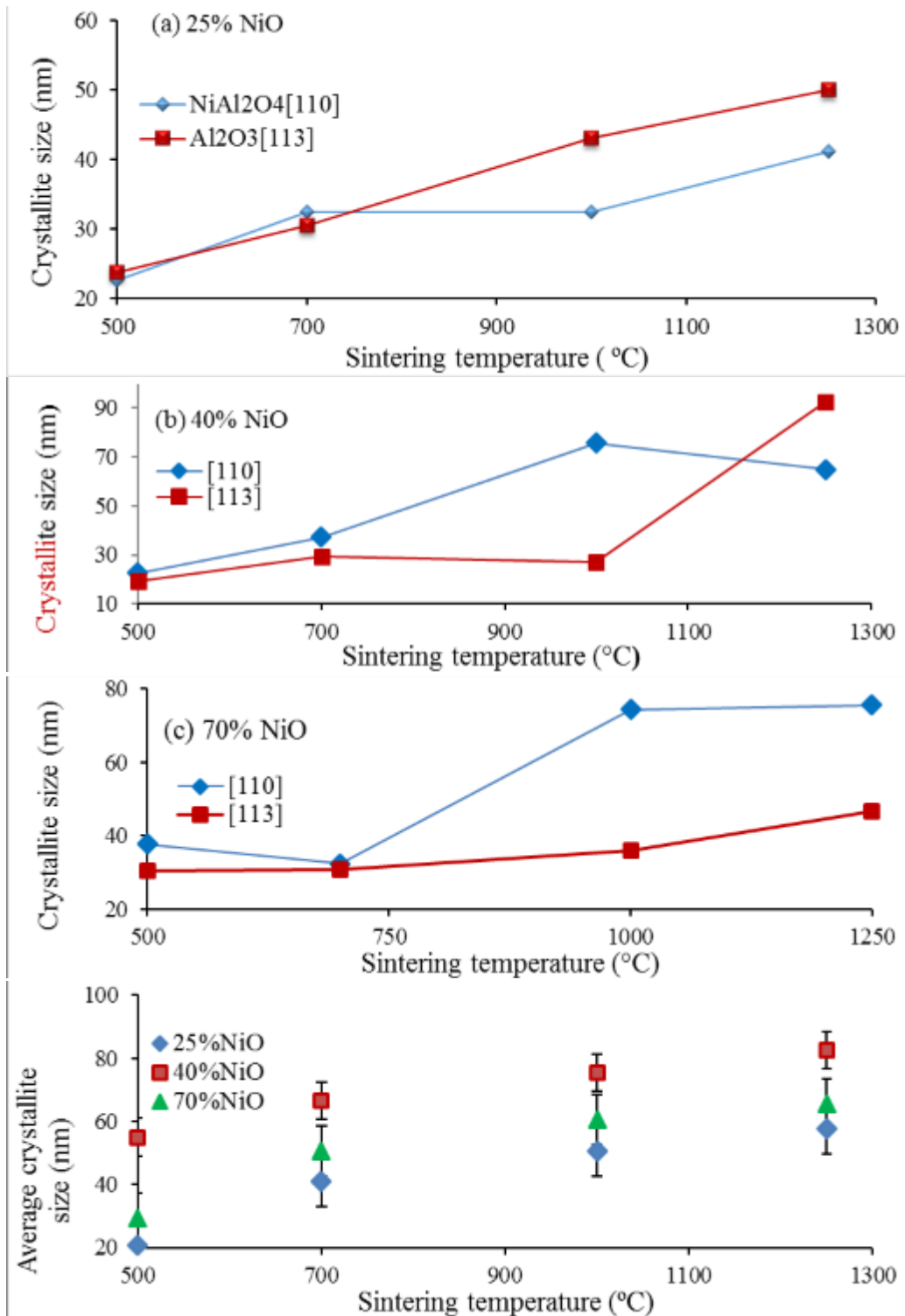


Figure 10. The crystallite size (a, b and c) and the Average crystallite size (d) as function of the sintering temperature and the NiO content.

al analysis was done on full sample surface viewed under 2000 X magnification with accelerating voltage of 15 kV, sampling time of 60 seconds and with a spot size of 50 nm. The overall spectrum of

the Al_2O_3 -NiO composites with different contents of NiO sintered at 1000 $^{\circ}C$ in air is shown in Fig. 8. The results show clearly the presence of Al, Ni and O, as expected for the NiO and Al_2O_3 con-

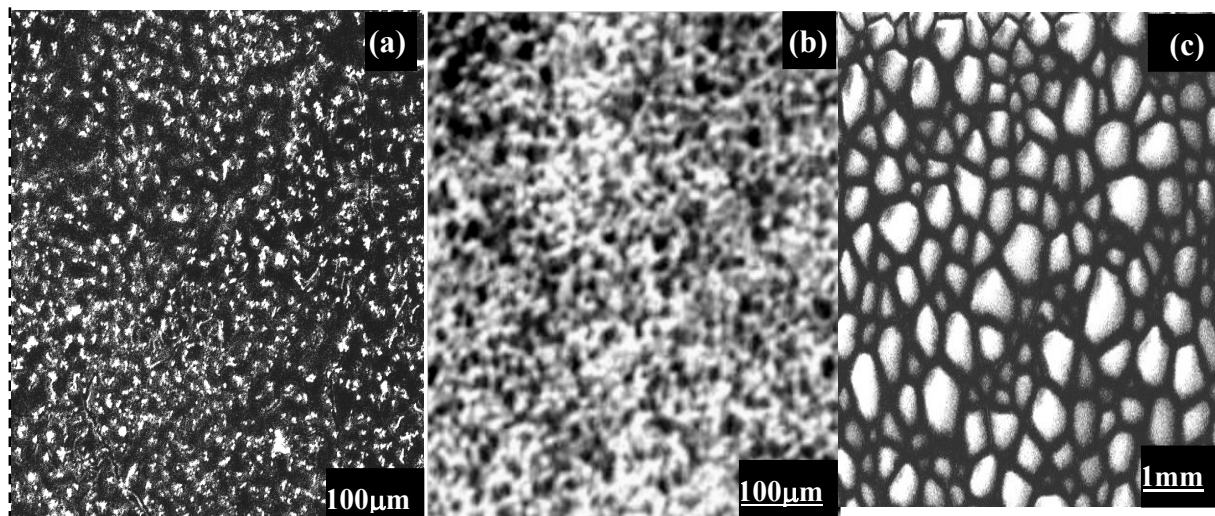


Figure 11. Surface morphologies by SEM of Al_2O_3 -40% NiO composites deposited at 150 V and sintered at 700 °C (a), 1000 °C (b) and 1250 °C (c)

firing hence that the powder mixture was composed entirely of NiO and Al_2O_3 . The copper peak was attributed to the impurities in the underlying nickel electrode.

3.3. The effect of sintering temperature on the composite properties

3.3.1. The effect of sintering temperature on composite crystallite size and orientation

The XRD patterns of the Al_2O_3 -NiO containing various NiO contents and annealed between 500 and 1250 °C for 5 h, are shown in Figs. 9a to 9c (peaks marked A correspond to Al_2O_3 , N to NiO and S to NiAl_2O_4).

For these various samples, a cubic nickel spinel (NiAl_2O_4) like phase is formed. The samples heated at 500 °C present a lower crystallinity, while the samples sintering at 1000 and 1250 °C are substantially crystalline and their diffraction patterns are relatively similar. From Fig. 9a to 9c, it is evident that Al_2O_3 -NiO films texturing is strongly dependent on the sintering temperature. The peaks intensity increases with the sintering temperature. However the number of peaks is reduced with the sintering temperature. The most important diffraction peaks of the composites have been observed for samples sintered at higher temperature (up to 1250 °C).

The crystallite size was calculated using the Scherrer's formula. The crystallite and the average crystallite size as function of the sintering temperature and NiO content are shown in Fig. 10a to 10d. The average crystallite size of the samples increases with the sintering temperature. In Fig. 10a (25% of NiO content), the main phases were Al_2O_3 and NiAl_2O_4 and the crystallite size of NiAl_2O_4 and Al_2O_3 could be obtained from the width of (110) and (113) diffraction peak respectively. According to Fig. 10a, the rate of the crystallite size of NiAl_2O_4 is lower than those of the crystallite size of Al_2O_3 between 500 °C and 1000 °C.

As shown in Fig. 10b (40% of NiO content), the sol phase is NiAl_2O_4 . The crystallite size of NiAl_2O_4 increased very slowly from 19 to 27 nm as the sintering temperature between 500 °C and 1000 °C, but increased rapidly from 27 to 92 nm between 1000 °C

and 1250 °C. Therefore the crystallite size of NiAl_2O_4 (110) decreased from 75 to 64 nm between 1000 °C and 1200 °C.

The crystallite size is measured in direction normal to the reflection plane, and, the increase in the crystallite size may be interpreted in terms of a columnar grain growth. This is mainly due to the increase of the particles agglomeration between at higher temperatures.

3.3.2. The effect of sintering temperature on composite microstructure

Fig. 11 shows the microstructure of fracture surfaces of Al_2O_3 -40% NiO composites sintered at various temperatures (700 °C, 1000 °C, 1250 °C). It can be noticed that the NiO particles (white color on the SEM images) were uniformly dispersed in the Al_2O_3 matrix (gray color), and there are a lot of pores for the sample sintered at 700 °C (Fig. 11a), a few pores for the sample sintered at 1000 °C (Fig. 11b) and no pores were seen on the micrograph when the sample is sintered at 1250 °C (Fig. 11c). However micrograph of sample sintered at 1250 °C clearly reveal that NiO grains are agglomerated. This reason is probably due to the fact that the NiO particles in the coating layer are very fine. According to the micrographs of the composites, it is evident that the particle grain size of NiO increases with the sintering temperature. This is mainly due to the particles agglomeration at high temperatures.

3.4. The effect of the applied voltage on composite weight gain and microstructure

During EPD, one of the most important parameters is the electric field, which is applied either through constant current density or constant voltage across the electrodes immersed in the suspension electrolyte. In agreement with Eq. (3), the deposit weight gain was found to increase with the deposition time and/or voltage. Composite samples were prepared at different applied voltages under similar conditions to evaluate the deposition weight gain. Results are shown in Fig. 12. It was found that, the weight gain of the composites is greatly affected by the increase in the applied voltage. In-

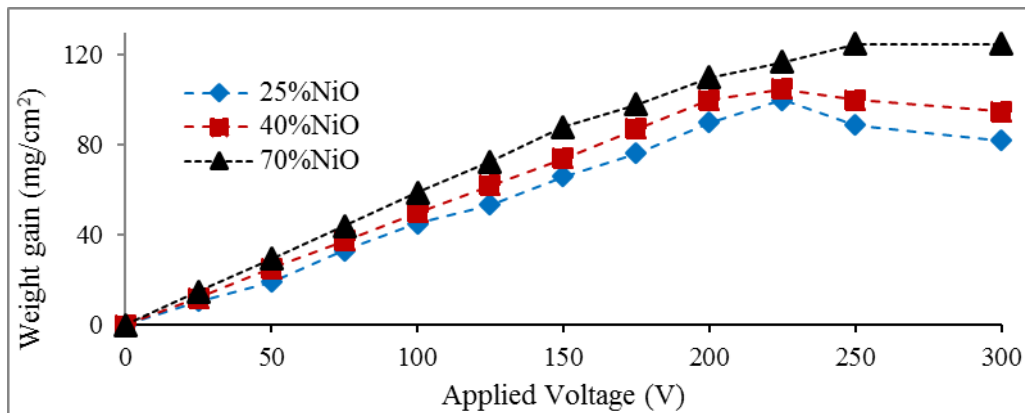


Figure 12. The deposition weight gain of composite containing variable NiO and sintering at 1000 °C as function of applied voltage.

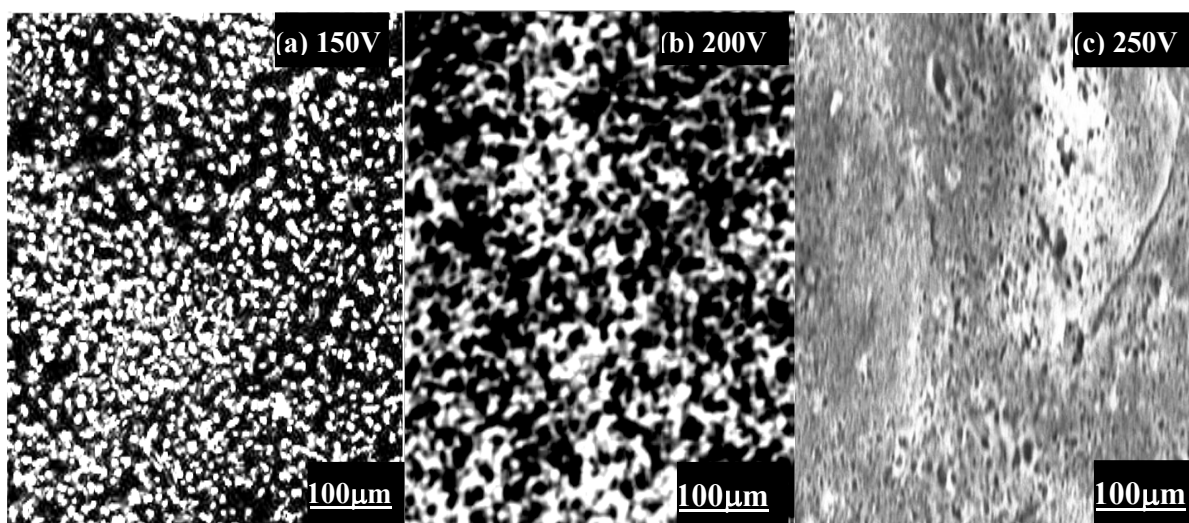


Figure 13. SEM pictures of the Al_2O_3 -40% NiO deposits sintering at 1000 °C at different applied voltages.

deed, when the applied voltage is less than 200 V, a linear weight gain is obtained and is in agreement with Eq. (4). Accordingly, the rate of growth of the films is similar for all the deposited composite materials. However, when the applied voltage is greater than 200 V, the weight gain of the composites containing 25 and 40% of NiO were reduced significantly in comparison to those of the composite containing 70% of NiO. The decrease in the deposition weight gain with the increase of the voltage at lower NiO contents can be attributed to the coarser Al_2O_3 particles with lower nobilities. Fig. 13 shows the SEM micrographs of Al_2O_3 -40% NiO composite, deposited by EPD at applied voltages of 150, 200 and 250 V on Ni substrate for 5 min. It can be noted that, when the voltage is greater than 150 V, a porous microstructure was visible on most parts. The big particles and higher porosity can be clearly observed on the composite prepared at constant voltage of 250 V. After the measurements of the deposited mass we have found that the deposition rate increases, of course, with the applied potential. The porous microstructure of the deposits is observed for applied voltage.

4. CONCLUSION

This work has shown that it is possible to fabricate Al_2O_3 -NiO composite particles by EPD from the mixtures of alumina and nickel oxide nanopowders in an ethanol-water solvent. It was also shown that the deposition weight gain increases with the NiO content. The thickness of the deposit can be easily controlled by the deposition time or NiO content. Microstructure studies have indicated that the NiO particles were uniformly dispersed on the grain boundaries and triple points of Al_2O_3 matrix. This illustrates clearly the advantage of the EPD for the synthesis of Al_2O_3 -NiO composite particles. When the NiO content increases, the particles distribution becomes more symmetric and homogenous forming thereby an interconnected network like-microstructure which inhibited grain growth of Al_2O_3 . This could help in the improvement of the mechanical properties of the composites. XRD studies have revealed that the composites possess the close crystallinity, and apart from Al_2O_3 and NiO, a cubic nickel spinel ($NiAl_2O_4$) like phase is formed and the average crystallite size of the samples increase with

the sintering temperature, mainly due to the particles agglomeration between at higher temperatures. However high applied voltage of the composite fabrication is not beneficial for the formation of homogeneous and crystalline composites at lower NiO contents ($\leq 40\%$). The composite deposited at high voltage exhibit porous microstructure. Future studies of these composites materials must focus on mechanical, electrical and selective optical properties measurements.

REFERENCES

- [1] S. Süzer, F. Kadirgan, H.M. Söhmen, A.J. Wetherilt, and I.E. Türe, *Solar Energy Materials and Solar Cells*, 52, 55 (1998).
- [2] T.C. Wang, R.Z. Chen and W.H. Tuan, *Journal of the European Ceramic Society*, 23, 927 (2003).
- [3] W.H. Tuan, H.H. Wu and T.J. Yang, *J. Mater. Sci.*, 30, 855 (1995).
- [4] T.S. Sathiaraj, R. Thangaraj, and O.P. Agnihotri, *Solar Energy Materials*, 18, 343 (1989).
- [5] G. Katumba, G. Makiwa, T.R. Baisitse, L. Olumekor, A. Forbes and E. Wäckelgård, *physica status solidi (c)*, 5, 549 (2008).
- [6] N. Nagarajan and P.S. Nicholson, *Journal of the American Ceramic Society*, 87, 2053 (2004).
- [7] M.K. Carpenter, R.S. Conell and D.A. Corrigan, *Solar Energy Materials*, 16, 333 (1987).
- [8] A. Hakim, J. Hossain and K.A. Khan, *Renewable Energy*, 34, 2625 (2009).
- [9] M.-S. Wu, M.-J. Wang and J.-J. Jow, *Journal of Power Sources*, 195, 3950 (2010).
- [10] T. Sekino, T. Nakajima, S. Ueda and K. Niihara, *Journal of the American Ceramic Society*, 80, 1139 (1997).
- [11] E. Kiš, R. Marinković-Nedučín, G. Lomić, G. Bošković, D.Ž. Obadović, J. Kiurski and P. Putanov, *Polyhedron*, 17, 27 (1998).
- [12] S.A. Makhlouf and K.M.S. Khalil, *Solid State Ionics*, 164, 97 (2003).
- [13] C. You, D.L. Jiang, and S.H. Tan, *Ceramics International*, 30, 813 (2004).
- [14] P. Sarkar and P.S. Nicholson, *Journal of the American Ceramic Society*, 79, 1987 (1996).
- [15] E. Harsanyi, "Coating radiant bodies such as thermionic valve cathodes", US1897902, 1933.
- [16] Y.-H. Qin, H.-H. Yang, X.-S. Zhang, P. Li, X.-G. Zhou, L. Niu and W.-K. Yuan, *Carbon*, 48, 3323 (2010).
- [17] K.M. Wu, P. Imin, A. Adronov and I. Zhitomirsky, *Materials Chemistry and Physics*, 125, 210 (2011).
- [18] L. Vandeperre, D.B.O. Van, F. Bouyer, J. Persello and A. Foissy, *J. Eur. Ceram. Soc.*, 17, 373 (1997).
- [19] B. Ferrari and R. Moreno, *Journal of the European Ceramic Society*, 17, 549 (1997).
- [20] H. Hadraba, K. Maca, and J. Cihlar, *Ceramics International*, 30, 853 (2004).
- [21] P. Sarkar, S. Datta and P.S. Nicholson, *Composites Part B: Engineering*, 28, 49 (1997).
- [22] I. Corni, M.P. Ryan and A.R. Boccaccini, *Journal of the European Ceramic Society*, 28, 1353 (2008).
- [23] B. Ouédraogo and O. Savadogo, *Journal of Scientific Research & Reports*, 2, 190 (2013).
- [24] H.C. Hamaker, *Transactions of the Faraday Society*, 35, 1940.
- [25] d.B.O.O. Van and L.J. Vandeperre, *Annu. Rev. Mater. Sci.*, 29, 327 (1999).